Mechanical Behavior and Constitutive Modeling of Cement–Bentonite Mixtures for Cutoff Walls

Mechanical behavior and constitutive modeling of cement-bentonite mixtures for cutoff walls

Luca Flessati[1], Gabriele Della Vecchia[2], and Guido Musso[3]

[1]Department of Civil and Environmental Engineering, Politecnico di Milano, Piazza Leonardo da Vinci 32 Milano, Italy

[2]Department of Civil and Environmental Engineering, Politecnico di Milano, Piazza Leonardo da Vinci 32 Milano, Italy Email: luca.flessati@polimi.it

[3]Department of Structural, Geotechnical and Building Engineering, Politecnico di Torino, Corso Duca degli Abruzzi 24 Torino, Italy

ABSTRACT

Cement-bentonite mixtures are commonly used to build cutoff walls which limit water flow and underground transport of pollutants. These artificial materials are employed due to their very low permeability and adequate shear strength and ductility. In this paper, experimental results about the microstructure and the mechanical behavior of three different cement-bentonite mixtures are presented. Specimens of these mixtures were subjected to oedometer and consolidated-undrained triaxial tests. These results were then used as a basis for the definition of a suitable constitutive framework. A quite good reproduction of the experimental results up to the peak strength was obtained using the classical Modified Cam Clay model, which could then be used satisfactorily when conventional analyses aimed at assessing the stability of cutoff walls are required. The reproduction of the strength degradation and the strains occurring in the post peak stage requires however a more advanced constitutive model. To this extent, Modified Cam Clay framework was enhanced by introducing some features commonly employed to reproduce the mechanical behavior of granular

materials. This model may be useful for the real scale analysis of more critical cases, when local failure mechanisms are likely to occur and may influence the functionality of the wall.

INTRODUCTION

In environmental geotechnics, barriers are often designed for seepage control and for the isolation of pollutants that may contaminate the groundwater. Cutoff walls are one of the most widespread solutions (Opdyke and Evans 2005; Joshi et al. 2010; Jefferis 2012; Royal et al. 2013; Soga et al. 2013; Carreto et al. 2016). **They are often built with cement-bentonite mixtures.** These artificial materials are used because of their very low permeability, but also because the construction processes they require are very simple. The cement-bentonite **mixture** in a slurry state fills a trench while this is excavated around the contaminated zone, remaining fluid along the whole excavation phase. Later on, the same mixture sets and hardens while left in the trench, forming a material with the required hydro-mechanical properties. According to Carreto et al. (2016), pure cement-bentonite mixtures are suitable for applications in which the required permeability is of the order of 10^{-8} m/s, i.e. for water seepage control. To further reduce the permeability and to increase durability with respect to chemicals in the groundwater, in many cases part of the cement is replaced with slag (Opdyke and Evans 2005; Royal et al. 2013; Soga et al. 2013; Royal et al. 2018).

Cement-bentonite mixtures are employed because of their low permeability, but a cut-off wall is also required to possess a shear strength roughly equivalent to the surrounding soils, and, more importantly, it should be sufficiently ductile so that cracks do not develop if the wall is subject to large strains under confined stress conditions. Thus, attention on the stress–strain behavior of containment walls is needed in order to avoid loss of cutoff performance. Typically, wall specifications call for a sample of the cement–bentonite mixture to accommodate a strain of at least 5% without cracking failure, despite in practice the ability of cement–bentonite to withstand these strains under drained conditions is rarely a problem, with values often in excess of 10% being achieved (Jefferis 1981). However, the brittle behavior shown by cement-bentonite mixtures at low confining stresses during

undrained triaxial loading (Soga et al. 2013; Carreto et al. 2016; Royal et al. 2018) may be critical for the barrier performance, as softening is related to the development of localized failures that could lead to preferential paths for water flow. While the hydraulic behavior of these mixtures has been investigated in detail, studies on the mechanical behavior have been mostly limited to the assessment of the material strength and constitutive models capable of assessing both material strength and strains at failure are lacking.

In this paper, **the results of an experimental study on the mechanical behavior of three different cement-bentonite mixtures are presented**, including oedometer and consolidated-undrained triaxial tests. The experimental results were exploited to evaluate the possible use of suitable constitutive mechanical models. The use of the Modified Cam Clay (MCC) model (Roscoe and Burland 1968) is first discussed. The MCC was chosen especially in light of its practicality, since (i) it requires a small number of constitutive parameters with clear physical meaning, (ii) the procedures to calibrate the constitutive parameters are well established and (iii) it is implemented in most numerical geotechnical codes. An enhanced model, introduced to improve the reproduction of aspects that are not very well handled by the MCC such as strength degradation, excess pore pressure evolution upon shearing and strain at failure, is then described. Such an advanced model is an original proposal and it was obtained by introducing in the MCC framework some features commonly employed to reproduce the undrained mechanical response of granular materials (Li and Dafalias 2000). This new model may be adopted in critical cases, when local failure mechanisms are likely to occur and may influence the functionality of the wall. The performance of both constitutive models was checked against both the experimental results reported in this work and against the ones in Carreto et al. (2016).

EXPERIMENTAL TESTS

In this section, the results of the experimental tests performed in the Geotechnical Laboratory of Politecnico di Torino are presented and discussed. After describing the procedure followed to obtain the cement-bentonite specimens, some photomicrographs of microstruc-

ture are presented together with experimental results of oedometer and triaxial tests.

Specimen preparation

The cement-bentonite slurries were prepared by mixing water, a sodium bentonite from Laviosa Mineraria (specific gravity 2.95, liquid limit 535%, plastic limit 75%) and Portland cement (CEM I 32.5N). Three different slurry compositions were considered (hereafter named CB4, CB5 and CB6) prepared by mixing in different proportions cement (C), bentonite (B) and water (W). The mass ratios used in the preparations are summarized in Table 1.

Preparation occurred in three steps: (i) water and bentonite were mixed by means of a laboratory mixer, (ii) after 24h, required for the bentonite hydration, cement was added and the slurry was mixed again and (iii) the mixtures were poured into cylindrical molds (Figure 1), having the size required to prepare the specimens for mechanical testing. The specimens were immersed in water, where they were cured for 28 days. During this last phase the specimens hardened and also consolidated under their self weight. Further details on the preparation of the specimens can be found in (Tarzia 2018).

After curing, the water content (w) and the specific gravity (G_s) were measured by means of standard laboratory tests (**ASTM (2019) Designation:D2216–19 and ASTM (2014) Designation:D854–14, repectively**). These values (Table 1) were employed to calculate the initial void ratio e_0 (Table 1) of the specimens of the different mixtures. Because of the presence of the cement and the reactions between water, bentonite and cement, the void ratio of the mixture is significantly lower than the one of the bentonite slurry (this one being equal to 22). As shown in Table 1, the higher the cement bentonite ratio, the lower the initial void ratio.

Investigation at the micro scale

The microstructure of specimens of the different mixtures was investigated by means of Scanning Electron Microscope (SEM) pictures, at magnifications ranging from 400 to 20000 fold the original. During SEM analyses, a vacuum condition must be imposed within the chamber and only dry, or nearly dry, specimens can be introduced. However, it has been

shown that the evaporation of water from Cement Bentonite occurring at room conditions has a significant impact on the material behavior, since it causes irreversible shrinkage (Trischitta et al. 2020) and the generation of cracks (Musso et al. 2020b). Limited experimental evidence also shows that such water evaporation reduces strength (Royal et al. 2018). All these evidences suggest that the fabric alters significantly when the mixture undergoes evaporation. To this extent, the SEM specimens were prepared following the same procedure used for the microstructural investigation of soil specimens (Delage and Pellerin 1984; Azizi et al. 2020). Dehydration was thus imposed through freeze-drying cycles, which, contrarily to evaporation, cause very limited changes to the original fabric.

The difference in terms of SEM images encountered between specimens of different mixtures was very small. For this reason, CB5 is selected as representative and SEM images of CB5 after curing are shown in Figure 2. At a 400 fold magnification (photograph in the left upper corner, bar length 300 microns) the microstructure appears to consist of roughly spherical elements, which are quite densely connected one with the other through a rather homogeneous fabric. These spherical elements have diameter of the order of a few tens of microns (silt size). A number of **pores** having a diameter of the order of about ten microns are present, as it can be appreciated at a 800 fold magnification (photograph in the right upper corner, bar length 100 microns). It is not possible to distinguish between the original clay platelets and the cementitious material.

Energy Dispersive X-ray microanalysis, run during SEM imaging on different parts of the specimen, detected atoms of Calcium, Silicon, Oxygen, Aluminum, Carbon and Magnesium (Figure 3). It was not possible to find a significant difference between the composition of solids on basis of their shape or size; furthermore the species that were found are bricks of the mineralogy of both cement and bentonite. No Sodium was detected, although this is a primary constituent of the original mineralogy of the bentonite. **On the contrary, Sodium was found to be abundant in the pore water, suggesting that cation exchange (Calcium for**

Sodium) might have occurred within the clay, consistently with the observations presented in (Kang et al. 2015). Due to the cement hydration reactions, the pore water within the specimens had a pH=12. Altogether, the high pH of the pore water and the prevalence of an exchangeable divalent cation (Calcium) in the bentonite structure, promote the aggregation of the bentonite particles into aggregates (van Olphen 1977). The "particles" observed at the 400 and 800 fold magnifications are then likely to be bentonite aggregates, more or less effectively "coated" by the cement. This justifies the large pores, which otherwise would be rather unusual for active clays such as bentonite.

The larger "silty elements" are found to be assemblages of hardened cement particles and aggregates of clay particles coated by cement, as it is appreciated at the 5000 fold magnification (left bottom picture). A field of **randomly** disposed ettringite needles, which do not form a clear reticular structure, grow between the particles and aggregates (right bottom picture).

On the overall, the observed fabric is very different from the one typical of bentonites, and despite the low permeability of the material, it is more similar to the one of a multiscale, silty-like, cemented material. Although the experimental observations here collected refer to specimens that were cured for 28 days, they are very consistent with the findings in Plee et al. (1990), which restricted the investigation to the first 24 hours of ageing.

Oedometer test results

The results of the oedometer tests performed on the three different mixtures, described in Tarzia (2018), are plotted in Figure 4 in the $e - \sigma'_v$ compression plane (being e and σ'_v the void ratio and the applied vertical effective stress, respectively). The experimental results allow identifying a vertical stress value corresponding to a sudden change in compressibility. This vertical stress, named in the geotechnical literature "preconsolidation pressure", is interpreted as a yield stress according to the generally adopted framework of elasto-plasticity. It is worth noting that the mixture tested is virgin from the mechanical point of view, implying that the yielding point is associated with the bonding provided by the cement

rather than to over-consolidation. According to Figure 4, the value of the preconsolidation stress increases with the cement content, being of the order of 30 kPa for the CB4 specimen and about 80 kPa and 140 kPa respectively for the CB5 and CB6 ones. **The experimental results also highlight that the slopes of the virgin loading branch is slightly affected by the cement content, with C_c values ranging from 3.5 for mixture CB4 to 3 for mixture CB6. The compression index C_c is defined as the slope of the virgin branch of the compression curve in the $e - \log \sigma'_v$ plane. The ratio between the compression index C_c and the swelling index ($C_s = 0.08$, defined as the slope of the unloading branch of the compression curve in the $e - \log \sigma'_v$ plane) is very large and on the average it is approximately equal to 40.** The role of cement appears more relevant if the compressibility is compared to the one of the pure bentonite. In that case, the measured values of C_c and C_s were equal to 7.9 and 3.9, respectively. This clearly puts in evidence that the presence of the cement significantly increases the stiffness and makes more evident the difference between mixture response during virgin loading and unloading. Interestingly, the slope of the initial branch of the compression curve (i.e. for vertical stress values lower than the preconsolidation one) is quite similar to the slope of the unloading branch. This may suggest that during these stages the variation of void ratio can be related to the same microstructural process, like the compressibility of cement-bentonite clusters. Moreover, the evidence that the elastic compressibility does not change after virgin loading, i.e when a spatial rearrangement of clusters certainly takes place, suggests that the bonds provided by the cement have not been significantly damaged during virgin loading.

Consolidated undrained triaxial tests

Consolidated undrained triaxial (TXCU) tests were run on the three different cement-bentonite mixtures (Tarzia 2018). The specimens were first isotropically consolidated at different confining pressure values. A backpressure was applied to ensure the full saturation of the specimens. **The confining pressure (p_c) is the difference between the cell pressure and the back pressure**. The experimental results obtained for p_c=20, 100 and

300 kPa are shown in Figures 5a-c. In particular, the results are plotted in (i) the $q-\varepsilon_a$ plane (being ε_a the imposed axial strain, $q = \sigma'_v - \sigma'_h$ the deviator stress whereas σ'_h is the horizontal effective stress, respectively), (ii) the $\Delta u - \varepsilon_a$ plane (being Δu the excess pore water pressure accumulated during shearing) and (iii) in the $q-p'$ plane (being $p' = (\sigma'_v + 2\sigma'_h)/3$ the average effective stress).

The experimental results reported in Figure 5a (p_c =20 kPa) put in evidence a similar response of specimens constituted of mixtures CB5 and CB6: the deviator stress increases monotonically up to an asymptotic value, whereas the initial increase of excess pore water pressure is followed by a decreasing branch, starting from an axial strain approximately equal to 1%. For both mixtures, the preconsolidation stress, identified along the compression curve (Figure 4), is significantly larger than the confining pressure applied during the consolidation stage of the triaxial test p_c: undrained shear is in this case applied to "highly overconsolidated" specimens. On the contrary, the preconsolidation stress for the CB4 specimen (as shown in Figure 4) is not significantly larger than the imposed p_c value: the specimen is in this case is "lightly overconsolidated" and both q and Δu are monotonically increasing with ε_a up to an asymptotic value.

The experimental results reported in Figures 5b and 5c are obtained for p_c values which are at least similar (Fig 4, CB6) or larger than the preconsolidation stress. In this case, the three specimens are normally consolidated and the type of undrained mechanical response seems not significantly affected by the C/B ratio. In the $q - \varepsilon_a$ plane a peak , followed by a decrease of the deviatoric stress, is evident. After the peak, excess pore water pressure remains constant. This implies that, analogously to what was obtained by Carreto et al. (2016), the decreasing branch of the effective stress path in the $q - p'$ plane is characterized by a slope equal to 3:1 (i.e. the same of the total stress path during the shear stage of triaxial tests).

A conventional interpretation of the strength of the different mixtures was

made in terms of Mohr-Coulomb envelopes, plotted in Figure 6. Towards the end of the tests, all the specimens of the different mixtures tended to a critical state condition. The ultimate (final) strength envelope was interpreted with the equation:

$$q = Mp' \tag{1}$$

For the CB4 mixture, it was found that the strength ratio q/p' increased monotonically with axial strain for all of the specimens, and there was no need to define a peak strength. On the contrary, for the CB5 and CB6 mixtures, the q/p' ratio showed a peak value at smaller strains before tending to the critical state at the end of the tests. This was particularly evident for the "highly overconsolidated" specimens tested at a confining pressure of 20 kPa. For these mixtures, a peak envelope was also defined, expressed as:

$$q = I + \eta_{max} p' \tag{2}$$

The parameters of Equations 1 and 2 can be related to the constant volume friction angle ϕ'_{cv}, the peak strength angle ϕ'_p and to the cohesion intercept c'_p (which might be of more common use in the engineering practice than M, η_{max} and I), through equations:

$$M = \frac{6 \sin \phi'_{cv}}{3 - \sin \phi'_{cv}} \qquad \eta_{max} = \frac{6 \sin \phi'_p}{3 - \sin \phi'_p} \qquad c'_p = I \cdot \frac{3 - \sin \phi'_p}{6 \cos \phi'_p} \tag{3}$$

The peak q/p' ratio of mixtures CB5 and CB6 decreases with the confining pressure, as expected to occur in soils as the degree of overconsolidation is reduced (see e.g. Atkinson and Bransby (1978)). The values of the strength parameters for the peak and the ultimate conditions are provided in Table 2. Interestingly, the friction angles slightly decrease as the cement/bentonite ratio

increases, while the cohesion increases with the cement/bentonite ratio.

CONSTITUTIVE MODELING

When dealing with cutoff wall behavior, chemo-hydraulic simulations are generally performed, neglecting the role of the mechanical response on the transport properties of the mixture. However, if deformation and stability issues are of concern, a mathematical formulation of the stress-strain response is needed. **In this section, the use of two different constitutive relationships to simulate the mechanical response of cement-bentonite mixtures, both of them in the framework of strain-hardening elasto-plasticity, is explored**. These are the standard Modified Cam Clay model (MCC) and an enhanced version of the MCC (CBC in the following), which was developed to improve predictions especially in the post peak branch.

Modified Cam Clay model

The Modified Cam Clay model is one of the most widespread constitutive models used in geotechnical engineering. It has been developed to simulate the mechanical behavior of saturated reconstituted clays, but its range of applicability has been extended to many other materials by properly adjusting the original formulation. The MCC model is an elastic-plastic model, characterized by isotropic hardening. When the stress state lies inside the yield locus or during unloading, material response is elastic: MCC assumes an isotropic non-linear elastic response, with a pressure dependent elastic bulk modulus (K) and a constant Poisson ratio (ν). The bulk modulus K is expressed as:

$$K = \frac{1 + e_0}{\kappa} p', \tag{4}$$

being κ is the slope of the unloading-reloading line in the $e - \ln p'$ plane.

In elasto-plasticity, the direction of the plastic strain increments is ruled by the plastic potential function (g). In associated plasticity, the yield function (f) and the plastic potential (g) are coincident. For the MCC, they are both ellipses in the $q - p'$ plane, expressed as:

$$f = g = \frac{q^2}{M^2} - p'(p'_s - p'), \tag{5}$$

where M and p'_s are the slope of the critical state line in the $q-p'$ plane and the hardening variable, respectively.

The increment of the hardening variable is defined according to the experimental evidence of material virgin compression along oedometer or isotropic paths:

$$\frac{\partial p'_s}{\partial \varepsilon^{pl}_{vol}} = \frac{1+e_0}{\lambda-\kappa} p'_s \tag{6}$$

being λ the inclination of the Normal Compression Line in the $e - \ln p'$ plane and ε^{pl}_{vol} the volumetric plastic strain.

By imposing the consistency conditions, the hardening modulus can be derived:

$$H = -\frac{\partial f}{\partial p'_s}\frac{\partial p'_s}{\partial \varepsilon^{pl}_{vol}}\frac{\partial g}{\partial p'} = (p')\left(\frac{1+e_0}{\lambda-\kappa} p'_s\right)(2p' - p'_s) \tag{7}$$

The hardening modulus, defining whether the material hardens ($H > 0$) or softens ($H < 0$), puts in evidence that hardening takes place when $p' > p'_s/2$ ("wet" clays according to Roscoe and Burland (1968)) whereas softening when $p' < p'_s/2$ ("dry" clays according to Roscoe and Burland (1968)). In case $p' = p'_s/2$, $H = 0$ and the material is at critical state, i.e. the material accumulates deviatoric plastic strains without changing its volume and state of stress.

Parameter calibration and model predictions

To calibrate the model, the values of four constitutive parameters (ν, κ, λ and M) and the initial value of the void ratio and the hardening variable (e_0 and p'_{s0}) have to be defined.

The initial void ratio values are taken from Table 1. The Poisson ratio value was assumed to be equal to 0.25, a realistic value for geotechnical analyses. The values of κ, λ and p'_{s0} were calibrated on the basis of the compression curve in oedometer conditions: κ was calibrated on the slope of the unloading branch, λ on the slope of the virgin branch and p'_{s0} where

the transition between the reloading and the virgin loading response takes place (Figures 7a-c). The MMC constitutive equations were integrated under oedometer stress paths (nil horizontal strains and an imposed vertical stress history) and the values of κ, λ and p'_{s0} were changed until a satisfactory agreement between the experimental results and the MMC prediction was obtained (Figure 7a-c).

The calibrated values of the relevant parameters of the MMC model for the three mixtures are listed in Table 3 (CB4, CB5 and CB6). M values were taken from Table 2.

The results of the undrained triaxial tests plotted in the $q - \varepsilon_a$ and the effective stress paths in the $q - p'$ plane were not directly exploited to calibrate the constitutive parameters, so that the experimental results in these planes may be employed for model validation. The comparison between experimental results (dotted liness) and the results obtained by numerically integrating the MMC model constitutive equations along an undrained triaxial stress path (solid lines) is reported in Figures 8-10. The MCC model satisfactorily reproduces the material mechanical response up to the peak deviator stress, but it is not able to reproduce the strength reduction. The dashed lines of Figures 8-10 will be commented in the following section.

A further verification on the validity of the MCC model to predict the behavior of these mixtures was done by simulating the tests reported in Carreto et al. (2016). In that paper the authors performed a series of isotropic compression and undrained triaxial tests on different cement-bentonite mixtures. For the sake of brevity, only one mixture composition (composition A in Carreto et al. (2016), W/B=28.6 and C/B=5.71) is hereafter discussed.

Analogously to the previous case, M was calibrated on final points of the effective stress paths and the Poisson ratio is assumed to be equal to 0.25, while e_0, κ, λ and p'_{s0} were calibrated on the isotropic compression test results. The values of the parameters are also summarized in Table 3.

The comparison between the experimental undrained triaxial test results corresponding

to p'_c=100, 200 and 400 kPa (dotted lines) and the results obtained by integrating MCC constitutive equations (solid lines) is reported in Figure 11. Also in this case, the reproduction of the experimental results is very satisfactory up to the peak deviatoric stress. The dashed line of Figure 11 will be commented in the following section.

It is worth mentioning that the mixture employed by Carreto et al. (2016) is different with respect to the one studied in this paper (Table 1). Even if the composition in terms of C/B ratio value is similar to the one corresponding to mixture CB6, the initial void ratio and the initial value of the hardening variable are similar to the one obtained for mixture CB4. Moreover, the values of λ and κ, associated with the material compliance, are larger with respect to the ones obtained for the mixtures studied in this paper. **These differences are likely due to the significantly larger W/B ratio value of the mixture employed by Carreto et al. (2016).**

Enhancement of MCC for cement-bentonite

Both the stress strain and the stress path plots in Figures 6-9 show that the MMC model allows a good estimation of the material strength and an adequate reproduction of the pre-failure behavior. Nevertheless, the reproduction of the post-failure behavior is rather poor. This is especially true with the specimens tested at higher confining pressures, which showed a noticeable loss of strength as the axial strains progressed. Remarkably, this is often is associated to localized failure, which would affect the integrity of the barrier causing preferential flow paths. It follows that the use of the MCC in the design of cutoff walls exposed to high mechanical solicitations might result unsafe, since it would not account for possible increase in the hydraulic conductivity of the barrier and loss of performance. A more advanced constitutive model should then be preferred.

To be able to reproduce the post-peak behavior, a novel strain hardening elastic-plastic constitutive model, hereafter named Cement Bentonite Constitutive model (CBC model), is introduced. In particular, the capabilities of the MCC were enhanced by using mathematical laws, related both to plastic flow and

hardening, inspired to existing relationships originally formulated for granular materials. This was motivated by the microstructural evidence discussed in the previous chapter and the experimental results of undrained triaxial tests. The clusters acting as solid grains convey the cement-bentonite mixture an undrained behavior that is very similar to the one of granular materials, namely: (i) progressive loss of strength when the material is in a 'normal-consolidated' loose state (i.e. when the void ratio is high with reference to the current confining pressure) and (ii) a ductile response when the material is in an 'over-consolidated' dense state (i.e. when the void ratio is low with reference to the current confining pressure). Notably, a similar approach was recently adopted by Musso et al. (2020a), to reproduce the mechanical behavior of unsaturated clayey silts.

For the sake of simplicity, the elastic law and the yield function are assumed to be the same of the MCC model, but the flow rule is assumed to be non-associated (i.e. the plastic potential and the yield function do not coincide). According to (Manzari and Dafalias 1997; Li and Dafalias 2000; Dafalias and Manzari 2004), the flow rule is expressed in terms of dilatancy d, defined as the ratio between the incremental volumetric plastic strain and the incremental deviatoric plastic strain. In particular, following Li and Dafalias (2000), dilatancy is assumed to depend not only on the stress obliquity $\eta = q/p'$ and M (like in the MCC model), but also on a scalar quantity ψ (Been and Jefferies 1985), named state parameter. In this paper, ψ is assumed to be a variable describing the distance (in term of void ratio) from the current material state (defined in terms of e and p') with respect to the corresponding critical state. It is defined as:

$$\psi = e - \left(\Gamma - \lambda \ln \frac{p'}{p_{ref}} \right) \tag{8}$$

where $p_{ref} = 1kPa$, whereas Γ and λ describe the critical state locus in the $e - p'$ plane. This latter is a straight line in the semilogarithmic $e - p'$ plane: λ represents its slope, whereas Γ is the (critical) void ratio for $p' = p_{ref}$. Analogously to what proposed in Li and

Dafalias (2000) for dilatancy evolution in sands, the following expression is adopted:

$$d = M \exp(g_1 \psi) - \eta, \tag{9}$$

where g_1 is a (positive) non-dimensional constitutive parameter. As for the hardening rule, it was again assumed to depend on η, M and ψ. The following plastic hardening modulus is thus proposed:

$$H = \left(p'_s \frac{1 + e_0}{\lambda - \kappa} \right) h_1 \left[\frac{M}{\eta} - \exp(h_2 \psi) \right] \tag{10}$$

where h_1 and h_2 are two (positive) non-dimensional constitutive parameters. In Equation 10, the term $(p'_s(1 + e_0)/(\lambda - \kappa))$ is the same appearing in the MMC hardening modulus (Equation 7), describing isotropic hardening as a function of plastic volumetric strains. A second contribution is then added, inspired by Li and Dafalias (2000), which takes into account η, M and ψ. This second term defines whether the material hardens ($H > 0$) or softens ($H < 0$). It is also worth mentioning that H can be nil either if (i) $M = \eta$ and $\psi = 0$ or (ii) if $M/\eta = \exp(h_2 \psi)$. In the former case, the material is at critical state, whereas in the second one the material is at failure.

Parameter calibration

To calibrate the CBC model, the values of eight constitutive parameters, as well as e_0 and p'_{s0}, have to be defined. Since the CBC model is intended to be an extension of the MMC model, the values of e_0, ν, κ λ, M and p'_{s0} were kept the same as before. For the sake of simplicity, it was assumed that g_1, h_1 and h_2 do not depend on the C/B ratio value.

The parameter h_1 may be calibrated independently from the other parameters on oedometer test results, relying on the fact that under oedometer compression neither the obliquity of the stress path nor the state parameter ψ change. For the sake of clarity, the influence of h_1 on the CBC model predictions is illustrated in Figure 12a. In the same figure the experimental results (corresponding to the CB5 specimen) are also reported. A satisfactory

agreement with experimental data was obtained using h_1=0.75.

The non-dimensional parameters g_1 and h_2 are related to the peak value in the $q - \varepsilon_a$ plane and to the slope of the post peak branch of the curve in the $q - \varepsilon_a$ plane, respectively. The influence of g_1 and h_2 on the CBC model predictions (where h_1=0.75 and Γ=11.5) is illustrated in Figures 12b and 12c, respectively. In the same figures, the experimental results (corresponding to the CB5 mixture) are also reported. The agreement between experimental data and model predictions is satisfactory for g_1=0.05 and for h_2=0.1.

The Γ values were calibrated on the experimental results, to correctly reproduce dilation and compaction obtained when the confining pressure was lower or larger than the preconsolidation stress, respectively.

The comparison between experimental triaxial test results (points) and model predictions (dashed lines) after parameter calibration (their values are reported in Table 4) is provided in Figures 8-11. In particular, the results corresponding to the mixtures CB4, CB5 and CB6 are reported in Figures 8, 9 and 10, respectively, whereas in Figure 11 the model predictions are compared with the experimental results of Carreto et al. (2016). **As it is evident, in all the cases considered the proposed constitutive relationship is capable of reproducing both the initial and the post-peak response: the maximum error in case mixture CB4, CB5 and CB6 are considered is smaller than 10%, whereas for mixture A of Carreto et al., 2016 is approximately 15% (for a confining pressure equal to 400kPa).** By summarizing, Figures 8-11 put in evidence that, with respect to MMC model, for the CBC model only one parameter more (Γ) has to be calibrated. The parameter values reported in Table 4 put in evidence that the Γ value is decreasing with C/B and it is not significantly affected by the W/B ratio value.

CONCLUDING REMARKS

In this paper, the results of experimental tests to investigate the mechanical behavior of cement-bentonite mixtures were discussed. Even though these mixtures are realized starting from bentonite slurries, the microstructure of these materials is dominated by silt-sized

elements composed of clay aggregates and cement, partially connected one to the other by means of cementation bonds. **The link between the peculiar microstructure of the cement-bentonite mixture and its mechanical responses here highlighted, with particular attention to the presence of clusters of particles and the bonding between them. Bonding mainly acts causing an increase in the yield stress that is not linked with previous stress history. The presence of clusters implies a response upon shearing that enhances dilation at low confining stresses and contraction at larger confining stresses, as generally obtained for cement-stabilized clays (Miura et al. 2001).** In fact, as suggested by the undrained triaxial test experimental results, at high confining stresses, the undrained response is characterized by a peak in the deviatoric stress, followed by a strength loss, in analogy with the behavior of loose granular materials. Moreover, from the experimental test results it can be concluded: (i) by increasing the water/bentonite mass ratio the initial void ratio and the compliance of the material increase, while the preconsolidation pressure decreases, (ii) by increasing the cement/bentonite mass ratio the initial void ratio decreases, the preconsolidation pressure increases, while the friction angle at critical state and the logarithmic compliance slightly decrease.

To reproduce the mechanical response of the mixtures, two different constitutive relationships were proposed: the Modified Cam Clay Model, and an original enhancement of the same model. Both the constitutive models can capture the previously cited dependence of the material properties on the mixture composition. The Modified Cam Clay model is suitable for reproducing the response up to the failure, but it cannot capture the post peak behavior. Therefore, this model may fruitfully be adopted in preliminary assessments, e.g. to verify whether, under in situ stress conditions, cracks may develop in cement bentonite cutoff walls. On the contrary, for more advanced analyses, e.g. in case the designers are interested to assess the crack size and geometrical distributions, the employment of the new constitutive relationship CBC is suggested. **The novel model was developed by**

joining the information at both the microstructural and laboratory scale in a unique framework, using conceptual tools widely accepted by the geotechnical community.

Data availability

Some or all data, models, or code that support the findings of this study are available from the corresponding author upon reasonable request. These include:

- numerical results of the simulations plotted in the manuscript;
- experimental data plotted in the manuscript;
- numerical code for the integration of the constitutive law.

Acknowledgments

The activity of the first author was financed in the context of the public administration agreement between Politecnico di Milano - Department of Civil and Environmental Engineering and the Italian Ministry of Economic Development, Direzione Generale per la Sicurezza anche Ambientale delle Attività Minerarie ed Energetiche – Ufficio Nazionale Minerario per gli Idrocarburi e le Georisorse – Programme Clypea, which is here gratefully acknowledged.

APPENDIX I. NOTATION

The following symbols are used in this paper:

B = Bentonite mass;

C = Cement mass;

c'_p = cohesion intercept;

d = Dilatancy;

C_c, C_s = Compression index and swelling index;

e, e_0 = Void ratio, initial void ratio;

f = Yield function;

G_s = Specific gravity;

g = Plastic potential function;

g_1 = Model parameter;

H = Hardening modulus;

h_1, h_2 = Model parameters;

I = Peak failure envelope intercept in the q-p' plane;

K = Elastic bulk modulus;

M = Slope of the critical state line in the $q - p'$ plane;

p' = Effective mean stress;

p_c = Confining pressure;

p_{ref}= Reference pressure (1 kPa);

p'_s, p'_{s0} = Hardening variable and initial value of p'_s;

q = Deviator stress;

W = Water mass;

w = Water content;

Γ = Critical void ratio for $p' = p_{ref}$;

Δu = Pore water pressure accumulated during triaxial test;

$\varepsilon_a, \varepsilon^{pl}_{vol}$ = Axial strain, volumetric plastic strain;

484 η_{max} = obliquity of the peak failure envelope in the q-p' plane;

485 κ = Unloading-reloading line inclination;

486 λ = Normal compression line and critical state line inclination;

487 ν = Poisson ratio;

488 σ'_h, σ'_v = Horizontal and vertical effective stress;

489 ϕ'_{cv}, ϕ'_p = Constant volume and peak friction angle ψ = State parameter

REFERENCES

Atkinson, J. H. and Bransby, P. L. (1978). *The mechanics of soils: an introduction to critical state soil mechanics*. McGraw-Hill Book Co.

Azizi, A., Musso, G., and Jommi, C. (2020). "Effects of repeated hydraulic loads on microstructure and hydraulic behaviour of a compacted clayey silt." *Canadian Geotechnical Journal*, 57(1), 100–114.

Been, K. and Jefferies, M. G. (1985). "A state parameter for sands." *Géotechnique*, 35(2), 99–112.

Carreto, J. M. R., Caldeira, L. M. M. S., and Neves, E. J. L. M. D. (2016). "Hydromechanical characterization of cement-bentonite slurries in the context of cutoff wall applications." *Journal of Materials in Civil Engineering*, 28(2), 04015093.

Dafalias, Y. F. and Manzari, M. T. (2004). "Simple plasticity sand model accounting for fabric change effects." *Journal of Engineering mechanics*, 130(6), 622–634.

Delage, P. and Pellerin, F. (1984). "Influence de la lyophilisation sur la structure d'une argile sensible du québec." *Clay minerals*, 19(2), 151–160.

Jefferis, S. (2012). "Cement-bentonite slurry systems." *Grouting and Deep Mixing 2012*, 1–24.

Jefferis, S. A. (1981). "Bentonite-cement slurries for hydraulic cut-offs." *Proceedings, Tenth International Conference on Soil Mechanics and Foundation Engineering, Stockholm, Sweden*, Vol. 1, 435–440.

Joshi, K., Kechavarzi, C., Sutherland, K., Ng, M. Y. A., Soga, K., and Tedd, P. (2010). "Laboratory and in situ tests for long-term hydraulic conductivity of a cement-bentonite cutoff wall." *Journal of geotechnical and geoenvironmental engineering*, 136(4), 562–572.

Kang, X., Kang, G. C., Chang, K. T., and Ge, L. (2015). "Chemically stabilized soft clays for road-base construction." *Journal of Materials in Civil Engineering*, 27(7), 04014199.

Li, X. S. and Dafalias, Y. F. (2000). "Dilatancy for cohesionless soils." *Geotechnique*, 50(4), 449–460.

Manzari, M. T. and Dafalias, Y. F. (1997). "A critical state two-surface plasticity model for

sands." *Geotechnique*, 47(2), 255–272.

Miura, N., Horpibulsuk, S., and Nagarj, T. (2001). "Engineering behavior of cement stabilized clay at high water content." *Soils and Foundations*, 41(5), 33–45.

Musso, G., Azizi, A., and Jommi, C. (2020a). "A microstructure-based elastoplastic model to describe the behaviour of a compacted clayey silt in isotropic and triaxial compression." *Canadian Geotechnical Journal*, 57, 1025–1043.

Musso, G., Zibisco, A., Cosentini, R. M., Trischitta, P., and Della Vecchia, G. (2020b). "Monitoring drying and wetting of a cement bentonite mixture with electrical resistivity tomography." *Proceedings of the 4th European Conference on Unsaturated Soil Mechanics, Lisbon, October 2020*.

Opdyke, S. M. and Evans, J. C. (2005). "Slag-cement-bentonite slurry walls." *Journal of geotechnical and geoenvironmental Engineering*, 131(6), 673–681.

Plee, D., Lebedenko, F., Obrecht, F., Letellier, M., and Van Damme, H. (1990). "Microstructure, permeability and rheology of bentonite - cement slurries." *Cement and Concrete Research*, 20(1), 45–61.

Roscoe, K. and Burland, J. B. (1968). "On the generalized stress-strain behaviour of wet clay." *In Engineering plasticity, Cambridge, UK: Cambridge University Press*, 535–609.

Royal, A., Makhover, Y., Moshirian, S., and Hesami, D. (2013). "Investigation of cement–bentonite slurry samples containing pfa in the ucs and triaxial apparatus." *Geotechnical and Geological Engineering*, 31(2), 767–781.

Royal, A., Opukumo, A., Qadr, C., Perkins, L., and Walenna, M. (2018). "Deformation and compression behaviour of a cement–bentonite slurry for groundwater control applications." *Geotechnical and Geological Engineering*, 36(2), 835–853.

Soga, K., Joshi, K., and Evans, J. (2013). "Cement bentonite cutoff walls for polluted sites." *Proceedings of the 1st international symposium on Coupled Phenomena in Geotechnical Engineering, Manassero et al. (Eds), Taylor Francis Group, London*, 149–165.

Tarzia, S. (2018). *Hydraulic behaviour of cement bentonite mixtures*. MSc thesis, Politecnico

di Torino (in Italian).

Trischitta, P., Cosentini, R. M., Della Vecchia, G., Sanetti, G., and Musso, G. (2020). "Preliminary investigation on the water retention behaviour of cement bentonite mixtures." *Proceedings of the 4th European Conference on Unsaturated Soil Mechanics, Lisbon, October 2020*.

van Olphen, H. (1977). *An introduction to clay colloid chemistry, for clay technologists, geologists, and soil scientists*. 2nd edition John Wiley & Sons, p. 318.

List of Tables

TABLE 1. Cement-bentonite mixture composition

	Mass ratio at preparation		Properties after 28 days of curing		
Mixture	Water/bentonite [-]	Cement/bentonite [-]	Water content w [%]	Specific gravity G_s [-]	Initial void ratio e_0 [-]
CB 4	18/1	4/1	306	2.88	8.8
CB 5	18/1	5/1	264	2.76	7.29
CB 6	18/1	6/1	230	2.72	6.25

TABLE 2. Ultimate and peak envelope parameters

	Critical state		Peak			
Mixture	$M[-]$	$\phi'_{cv}[^\circ]$	$\eta_{max}[-]$	$I[kPa]$	$\phi'_p[^\circ]$	$c'_p[kPa]$
CB 4	2.00	49.00	-	-	-	-
CB 5	1.96	47.75	2.03	15	49.30	7
CB 6	1.84	44.87	1.82	17	44.36	9

TABLE 3. Modified Cam Clay parameters

	e_0 [-]	ν [-]	κ [-]	λ [-]	M [-]	p'_{s0} [kPa]
CB4	8.8	0.25	0.06	1.5	2	30
CB5	7.29	0.25	0.06	1.35	1.96	65
CB6	6.25	0.25	0.06	1.2	1.84	110
mixture A Carreto et al. (2016)	8.58	0.25	0.09	1.45	2	25

TABLE 4. Constitutive model parameters

	e_0 [-]	ν [-]	κ [-]	λ [-]	M [-]	p'_{s0} [kPa]	g_1 [-]	h_1 [-]	h_2 [-]	Γ [-]
CB4	8.8	0.25	0.06	1.5	2	30	0.05	0.75	0.1	12.8
CB5	7.29	0.25	0.06	1.35	1.96	65	0.05	0.75	0.1	11.5
CB6	6.25	0.25	0.06	1.2	1.84	110	0.05	0.75	0.1	10.2
A of Carreto et al. (2016)	8.58	0.25	0.09	1.45	2	25	0.05	0.75	0.1	11

List of Figures

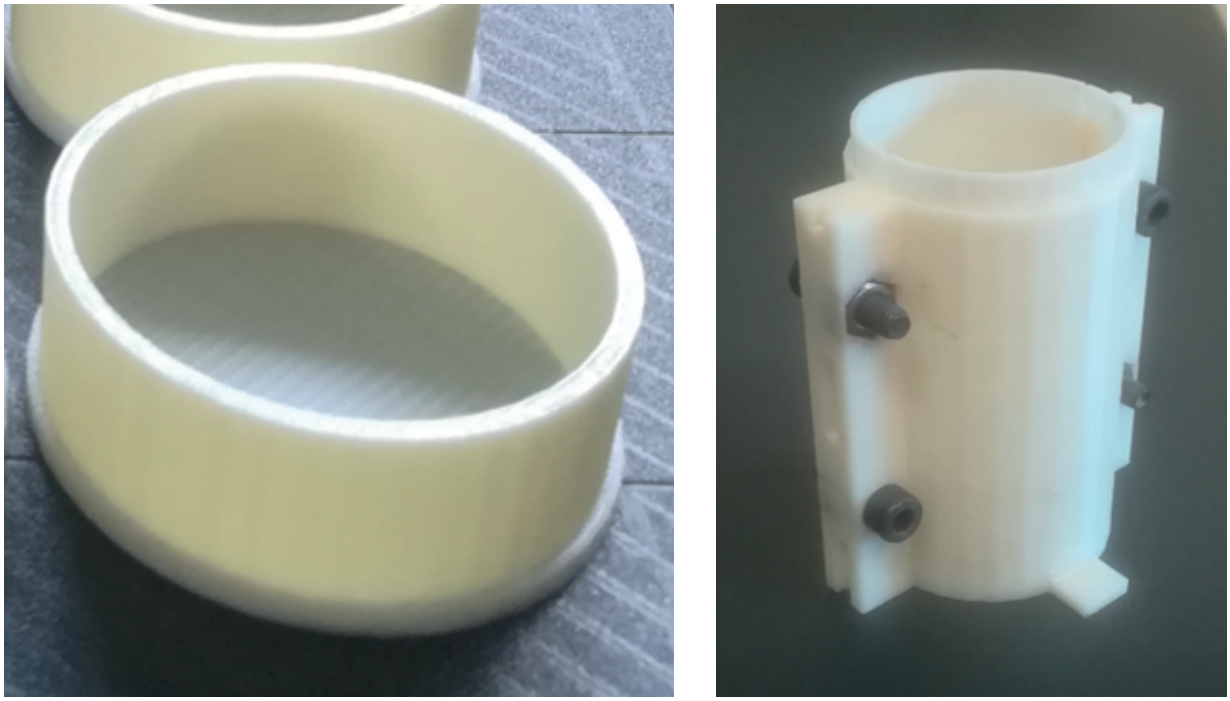

Fig. 1. Molds for the preparation of specimens for oedometer testing (left, internal diameter 50.5 mm and height 20 mm) and for triaxial tests (right, internal diameter 38.1 mm and height 76.2 mm)

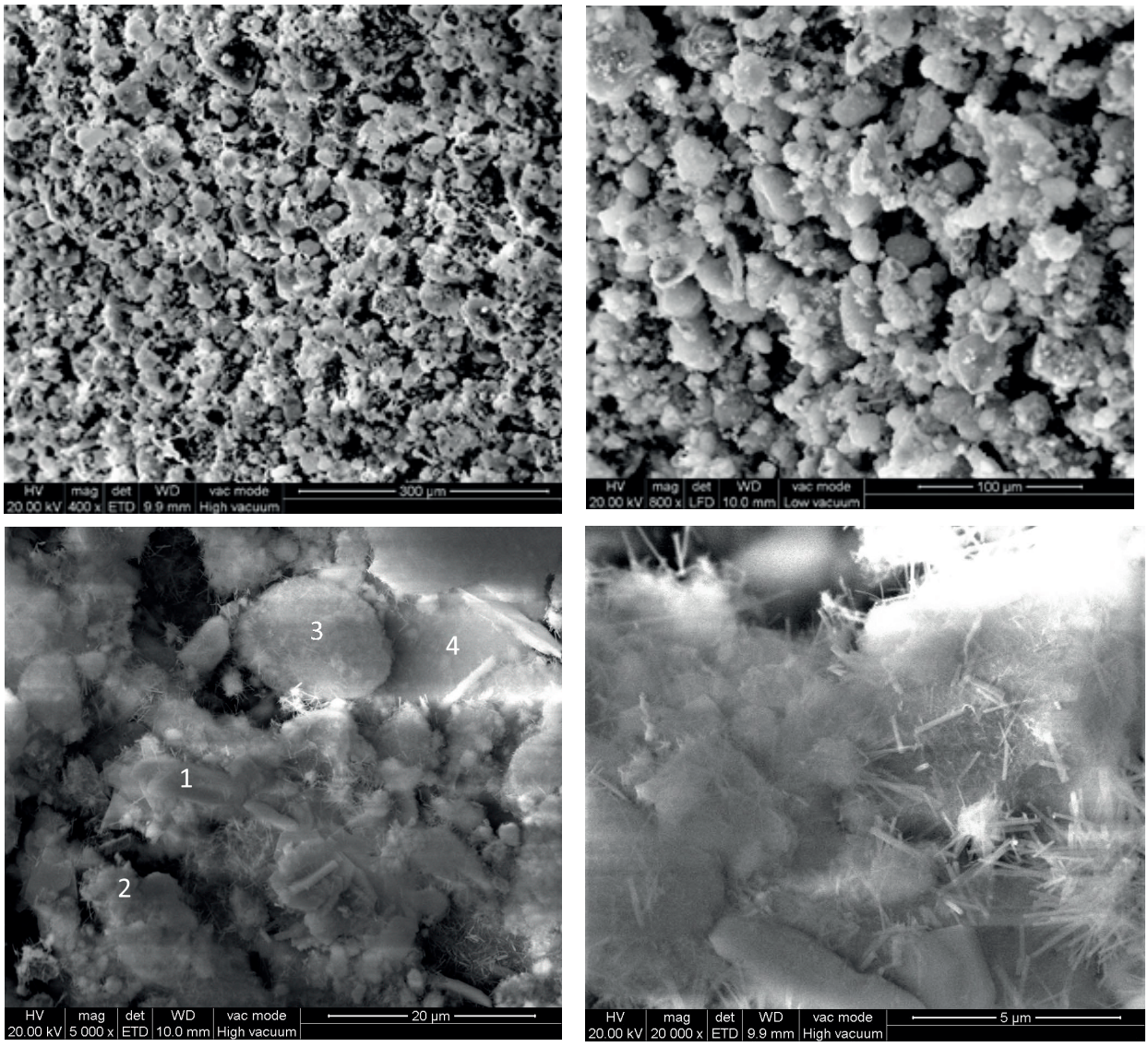

Fig. 2. SEM images at different magnifications of a CB5 specimen after 28 days of curing

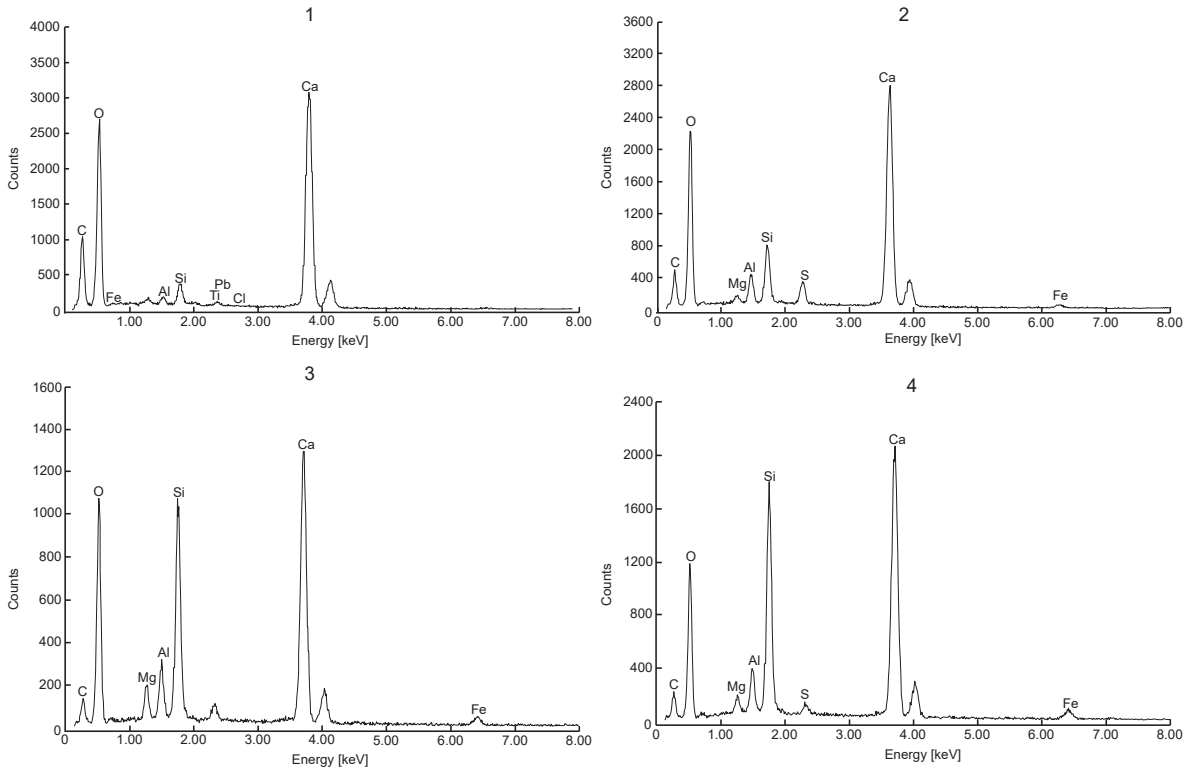

Fig. 3. Atomic composition detected during SEM testing through Energy Dispersive X-ray microanalysis. Numbers above each spectrum refer to the position in the bottom left image of Figure 2

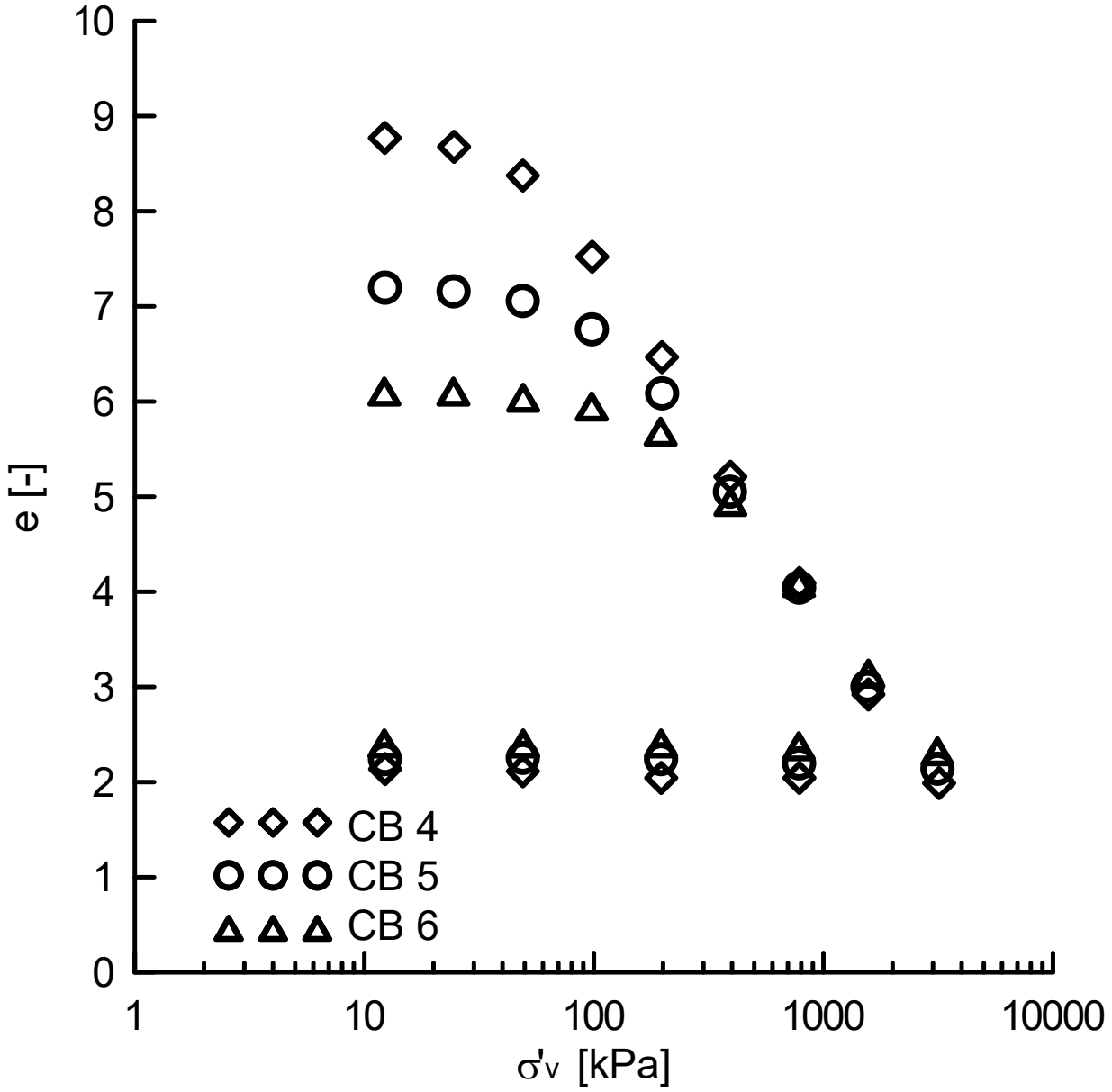

Fig. 4. Experimental compression curves in oedometer for the three cement-bentonite mixtures

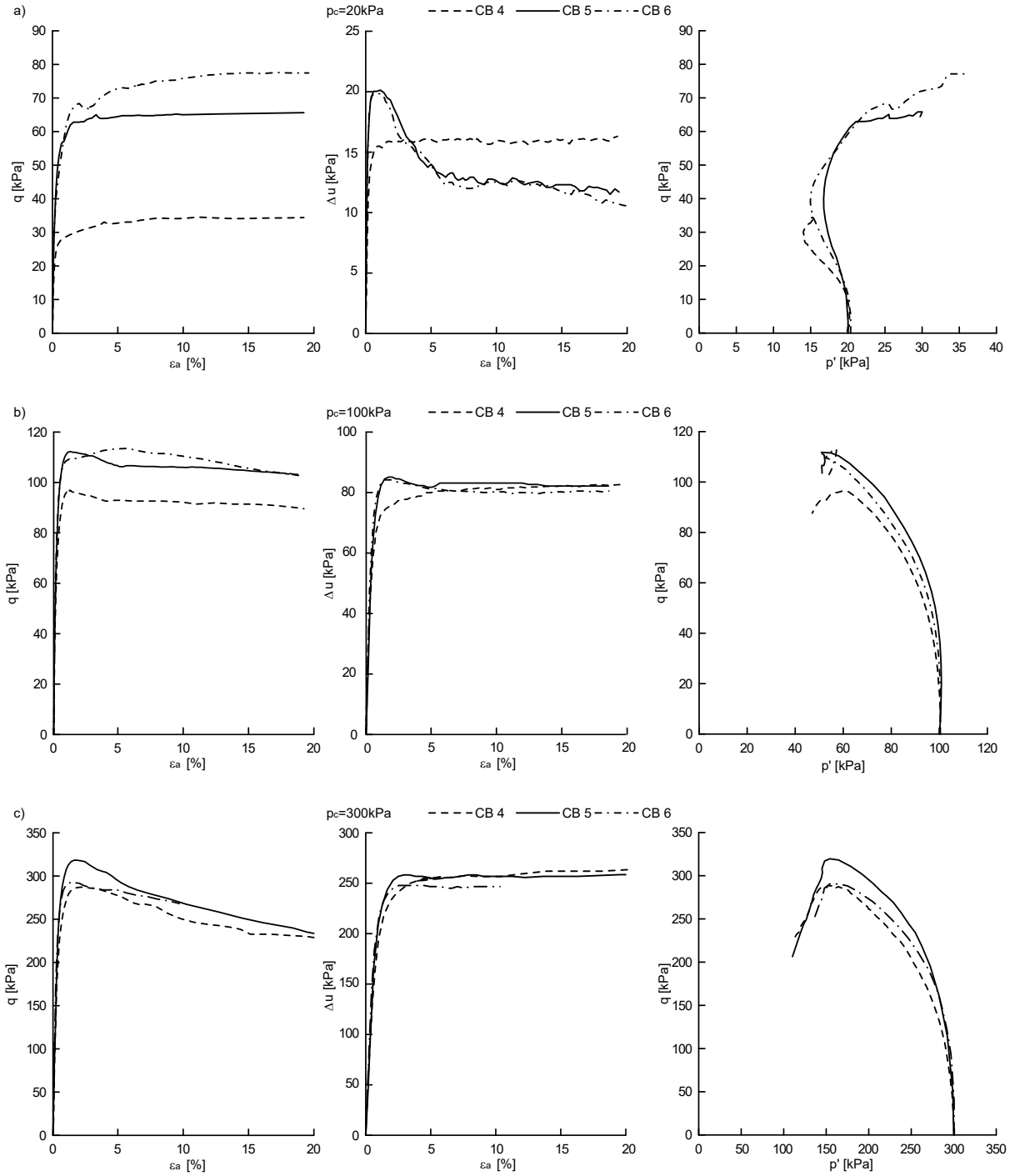

Fig. 5. TXCU test results for confining pressure equal to a) 20kPa, b) 100kPa and 300kPa

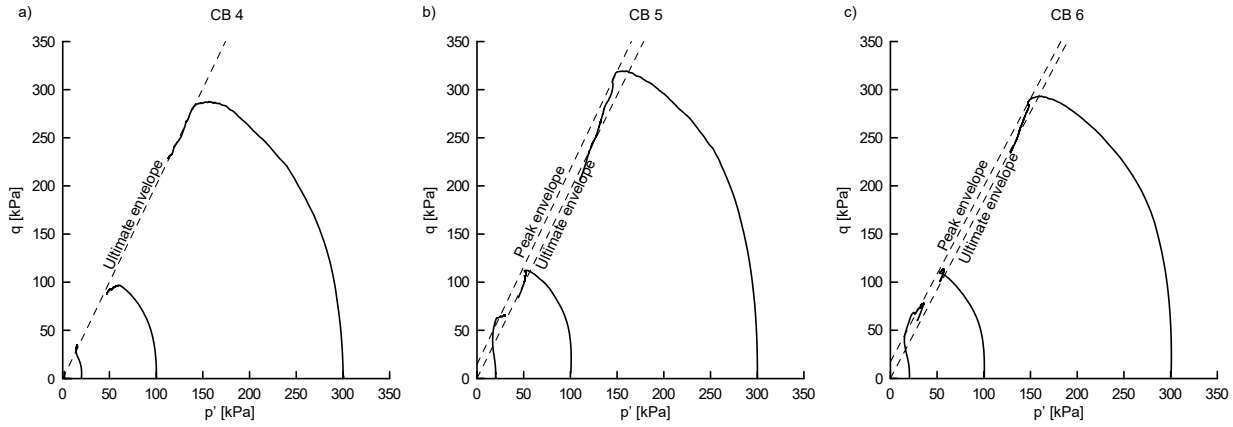

Fig. 6. Experimental determination of peak and ultimate envelope: a) CB4, b) CB5 and c) CB6

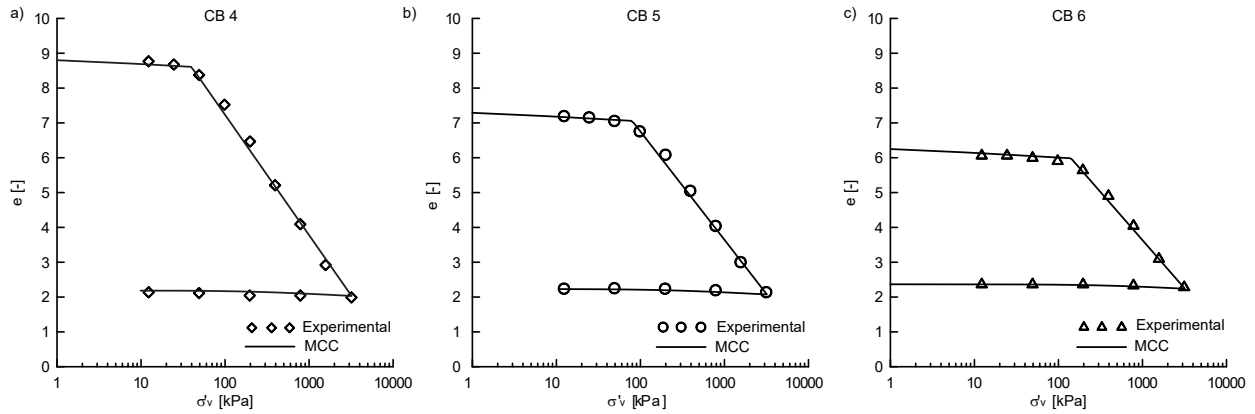

Fig. 7. Calibration of the MMC model parameters in the $e - \sigma'_v$ plane: a) mixture CB4, b) mixture CB5 and c) mixture CB6

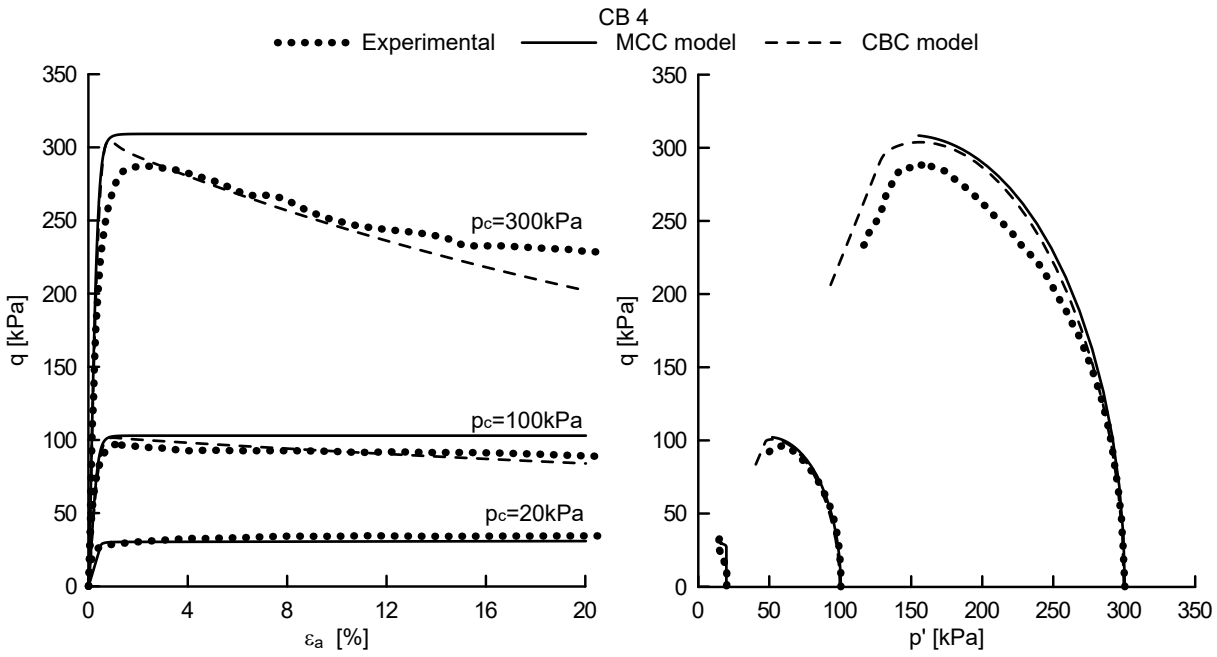

Fig. 8. Comparison between experimental results and constitutive model prediction (mixture CB4)

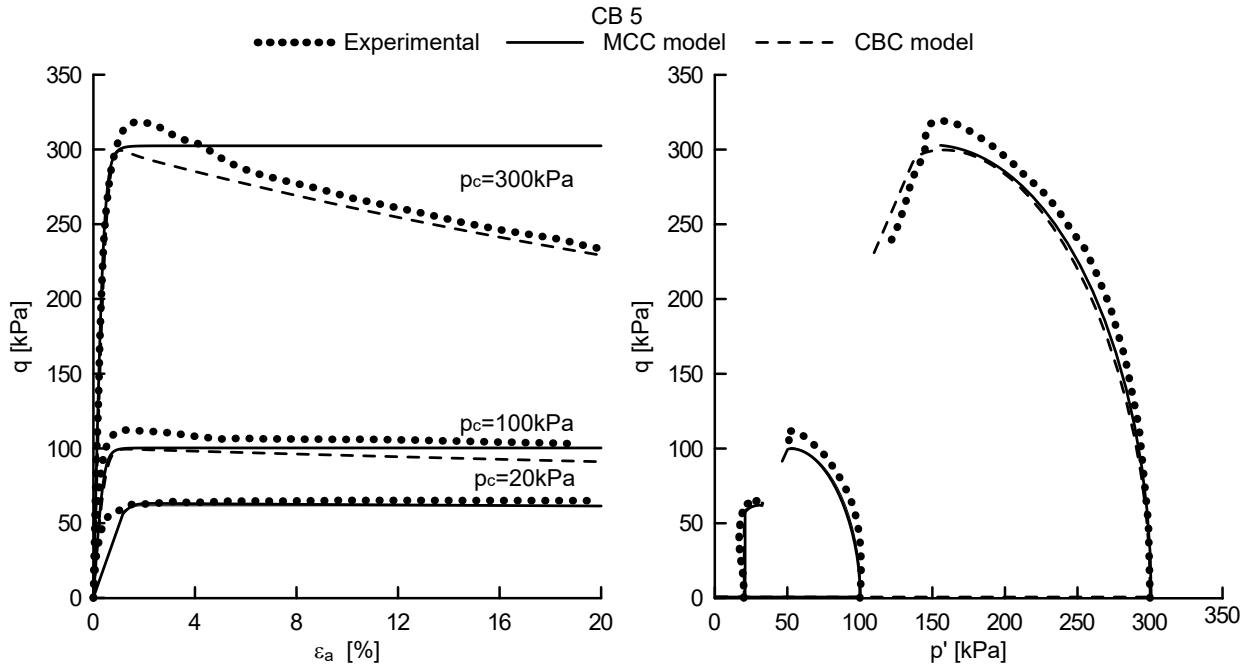

Fig. 9. Comparison between experimental results and constitutive model prediction (mixture CB5)

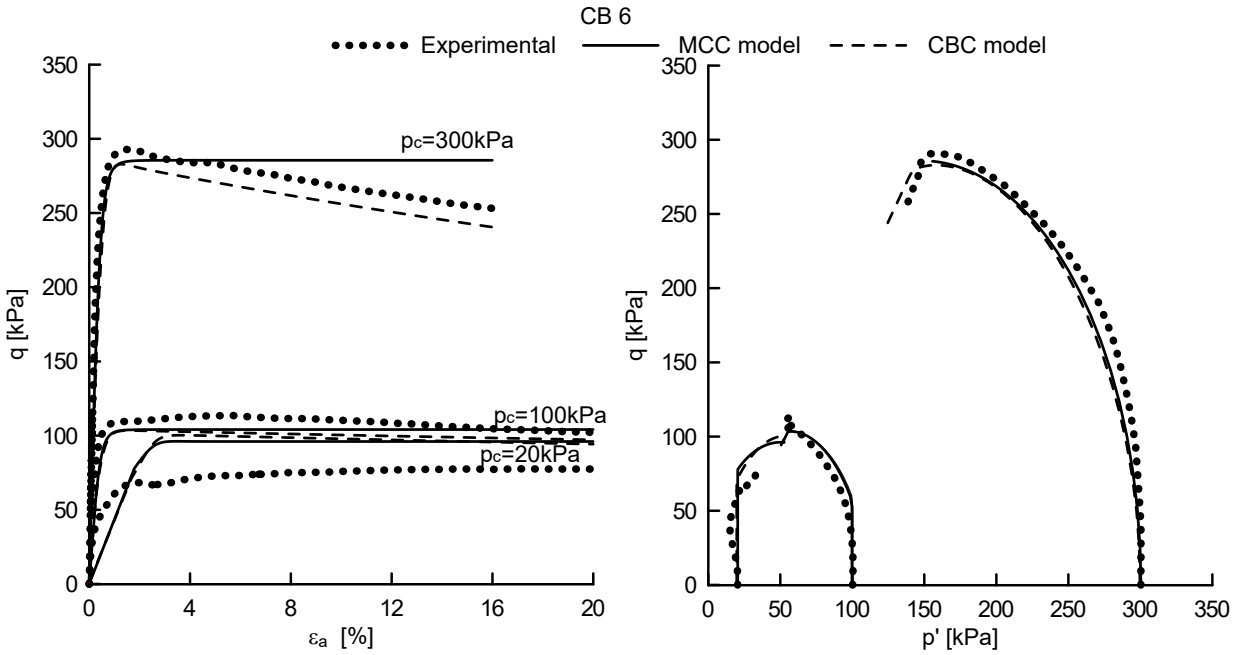

Fig. 10. Comparison between experimental results and constitutive model prediction (mixture CB6)

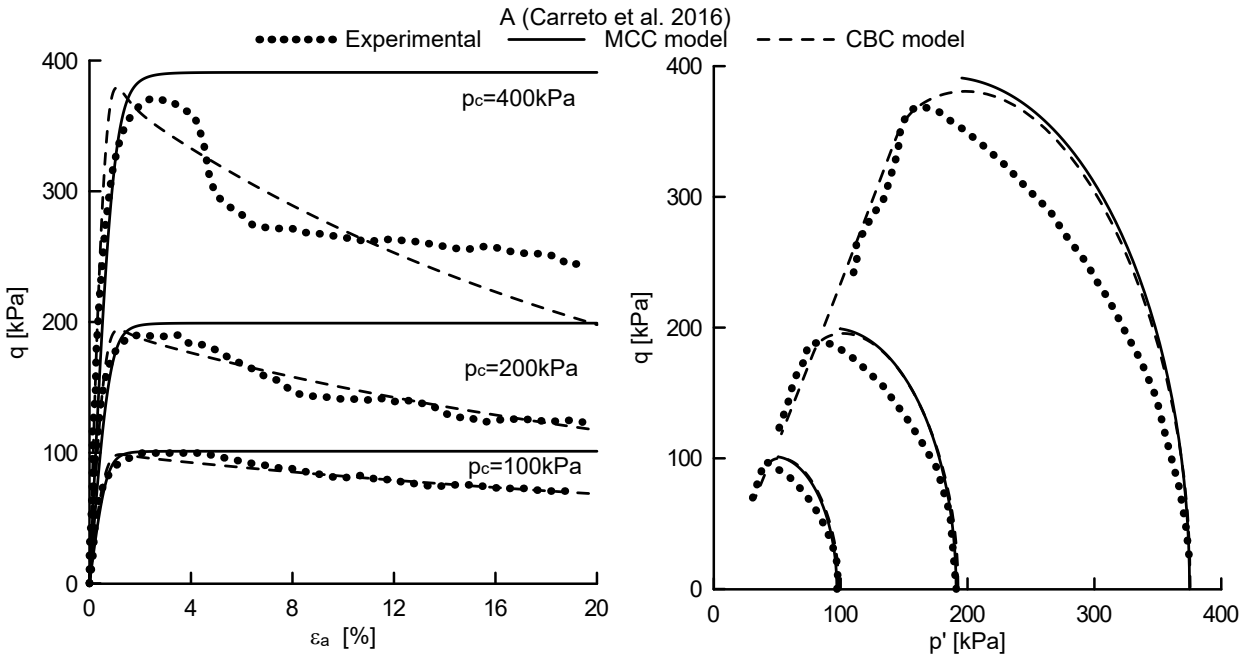

Fig. 11. Comparison between experimental results and constitutive models prediction (mixture A in Carreto et al. (2016))

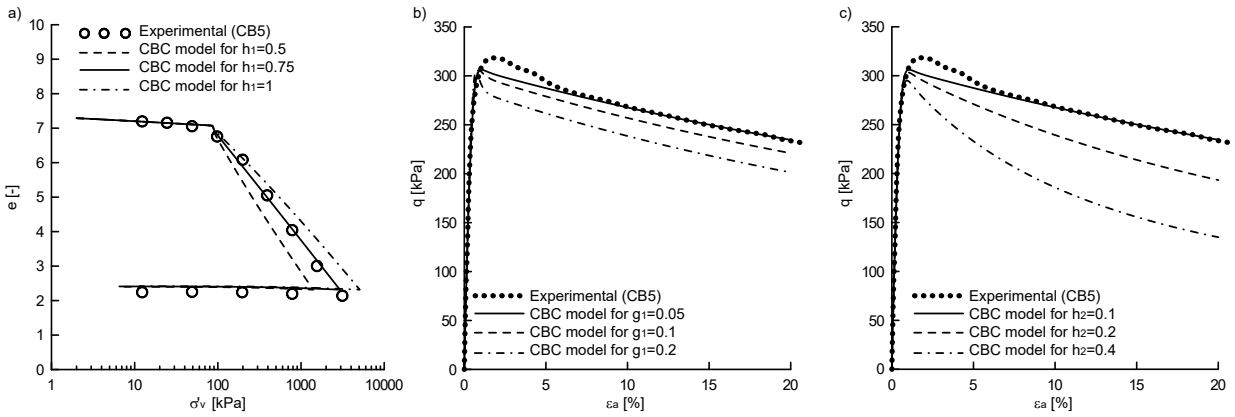

Fig. 12. Calibration of the parameters of the CBC model: a) h_1, b) g_1 and c) h_2